Sol-gel route: An original strategy to chemically stabilize proton exchange membranes for fuel cell

N. Huynh, J.P. Cosas Fernandes, P.A. Bayle, M. Bardet, Éliane Espuche, J. Dillet, Jean-Christophe Perrin, Assma El Kaddouri, O. Lottin, Vincent Mareau, et al.

Sol-Gel route: an original strategy to chemically stabilize proton exchange membranes for fuel cell

N. Huynh[1-3], J.P. Cosas Fernandes[1], P.A. Bayle[2], M. Bardet[2], E. Espuche[3], J. Dillet[4], J.-C Perrin[4], A. El Kaddouri[4], O. Lottin[4], V.H. Mareau[1], H. Mendil-Jakani[1], L. Gonon[1*]

[1]Univ. Grenoble Alpes, CEA, CNRS, IRIG-SyMMES, 38000, Grenoble, France

[2]Univ Grenoble Alpes, CEA, IRIG-MEM, 38000 Grenoble, France

[3]Université de Lyon, Université Lyon1, UMR CNRS 5223, Ingénierie des Matériaux Polymères, F-69622 Lyon, France

[4]Laboratoire d'Energie et de Mécanique Théorique et Appliquée (LEMTA) UMR CNRS / Université de Lorraine 7563, Nancy, France

We present the elaboration, *via* a Sol-Gel (SG) route, of a new generation of hybrid membranes for PEMFC applications, in order to improve their performances and durability. The strategy was to create, within a commercial sPEEK membrane, a reactive SG phase able to reduce the oxidative species generated during FC operation and to improve the proton conductivity. The SG content is adjusted by tuning the SG precursors/sPEEK ratio used for the impregnation step. Raman analyses show that a uniform distribution of the SG phase in the membrane section is obtained when NMR analyses demonstrate its high extent of condensation, and reveal the structuring effect of the sPEEK membrane on the SG phase at the nanoscale. The membranes exhibit a better liquid water uptake and proton conductivity than pristine sPEEK membrane up to a SG uptake of 18%, with a gas permeability slightly higher than sPEEK but still lower than the benchmark Nafion. H_2O_2 accelerated aging tests evidenced the ability of the SG phase to prevent the oxidative degradation of sPEEK. Finally, the FC operability tests showed better and more durable performances for the hybrid membranes, without any increase of the gas permeability during operation.

Key words: PEMFC, hybrid membranes, sol-gel, fuel cell, aging, antioxidant

* Corresponding author.
E-mail address: Laurent.gonon@univ-grenoble-alpes.fr

1 Introduction

Proton Exchange Membrane Fuel Cell (PEMFC) is a promising technology for converting hydrogen into electrical energy. This work focuses on the issues related to the PEM at the heart of the device, in the membrane electrode assembly (MEA). The challenge is to develop a PEM operating at high temperature (100-150°C)[1–5] and therefore at low relative humidity (10-50%) to improve performances and catalysts tolerance against gaseous poisoning. In addition, this membrane should withstand a lifetime of more than 8000/50000h[†] for transport and stationary applications respectively.

Two processes limit the PEM lifetime during FC operation[6–10]: chemical degradation and physical aging. Chemical degradation is caused by reactive radical species and hydrogen peroxide (H_2O_2) leading to polymer chain scission and a loss of the membrane's mechanical properties. Physical degradation results from the compressive forces applied to the membrane by the bipolar plates and is enhanced (i) by start/stop cycles (swelling/drying) associated to creep leading to a permanent membrane thinning up to pinhole formation (ii) when the FC operates above the glass transition temperature (T_g) of the membrane [7,8,11].

Notwithstanding intense research efforts, yet, no membrane can satisfy all the required specifications. Perfluorinated ionomers [3,12–14], known for their excellent chemical stability, loose most of their proton conductivity (if not properly hydrated) and mechanical properties above 80°C. Conversely, if the sulfonated polyaromatic polymer electrolytes show better thermomechanical stability, their proton conduction and their chemical stability are generally low[1–4,6–9,12].

In the past decades, different strategies were explored to address these issues[2–4,6–10,15,16]: chemical modifications, physical reinforcement and addition of a chemical stabilizer. Chemical modifications include:

- chemical crosslinking of the polymer [17],
- stabilization of the most sensitive group of the backbone[18,19],
- the design of novel block-copolymers (BCPs)[20–22],

[†] DOE 2015 HTAC Annual Report – August 2016

- Interpenetrated Networks[23–25] (IPN).

However, improving thermo-mechanical properties usually results into a drop of the proton conductivity due to a negative impact of the aforementioned strategies on sulfonated groups content and/or membrane nanostructure (phase demixing for IPN strategy for example).

Physical modifications[26,27] include membrane annealing to increase their crystallinity (to achieve lower chain mobility above T_g)[28,29], uniaxial stretching[11,27,29,30] to increase the polymer chain packing, and finally addition of a physical reinforcement like porous sheet of PTFE[31], polymer (nano)fiber mats[16,32–35] or nanoparticles (NPs) either by adding preformed nanofillers or by using a sol-gel (SG) process[17,36–39] to generate the nanofillers within the membrane. These technics allow improving the dimensional stability and durability of composite membranes when subjected to mechanical stresses.

In addition, the use of stabilizing additives against chemical degradation of PEM is investigated since 2005[10,26]. Two pathways are explored: the addition of H_2O_2 decomposition catalyst and the use of radical scavengers, which can be reversible (auto-regenerated in operating FC) or not (sacrificial compounds). H_2O_2 decomposition catalyst are metal oxide[40] (CeO_2, TiO_2…) or heteropolyacids[41]. Radical scavengers are metal NPs[42] (Au, Pd…), metallic ions (Ce^{3+}, Mn^{2+}…)[43–45], or organic antioxidant (α-tocopherol, terephtalic acid…)[35,46–48].

For both pathways, issues arise from the introduction, dispersion and possible elution in the exhaust water of these additives during FC operation, as well as their impact on the proton conductivity, mechanical properties and permeability of the membranes. These drawbacks can be mitigated by combining the use of stabilizing additives with SG chemistry[37,49,50]. As shown by Mauritz[36–39], the polar/nonpolar nanophase-separated morphologies of sulfonated membranes can act as a template directing SG hydrolysis / polycondensation of inorganic alkoxides. A functional SG phase can be introduced while maintaining the nanophase segregation of the pristine membrane (impregnation of the host membrane instead of membrane casting). Of course, as only a limited amount of additive can be introduced, the lifetime of the membrane cannot be infinite. However, a limited lifetime can be sufficient if it corresponds to the required lifetime for the application (the sacrificial stabilization strategy is

regularly used for polymer materials). In addition, the amount of SG phase has to be limited to avoid any detrimental effect on conductivity, gas permeability and water sorption.

Herein, this hybridization process is applied to sPEEK membranes. Indeed sPEEK is an attractive polyaromatic ionomer for high operating temperatures due to its excellent thermomechanical properties[51]. However sPEEK is very prone to chemical oxidation during FC operation [52–54]. It is therefore useless in its pristine form due to its short lifetime [52,53] (hundreds of hours *vs.* tens of thousands of hours for a Nafion membrane) but an ideal candidate to rapidly assess the stabilization strategy. A SG phase was therefore grown by self-condensation of (3-mercaptopropyl) trimethoxysilane (MPTMS) inside the sPEEK host membrane, with the aim to reduce the oxidative species generated in FC and therefore protect the sPEEK. Indeed, the mercapto groups carried by the SG phase can be oxidized up to the formation of sulfonated groups[55–58]. MPTMS has already been used to increase the proton conductivity of PEM after H_2O_2 oxidation of the mercapto into sulfonated groups [55–58], but never to neutralize the oxidative species generated in FC and therefore to protect the membrane from chemical aging.

This paper is focused on the membrane preparation conditions which have been optimized to obtain the most promising membranes (SG uptake and structure). Then, the functional properties (gas permeability, water sorption, proton conductivity and chemical stability under H_2O_2 accelerated aging tests) of the hybrid membrane as a function of the SG content are presented.

2 Experimental

2.1 Materials

sPEEK (sulfonated polyetheretherketone) membranes with an IEC of 1.34 meq g^{-1} were purchased from Fumatech. The sol-gel precursor, (3-mercaptopropyl)trimethoxysilane (MPTMS) was purchased from Aldrich (CAS n°4420-74-0).

2.2 Membrane fabrication process

Prior to impregnation, the host sPEEK membranes were re-acidified in a 1M HCl solution at room temperature for 4 hours, triple rinsed with pure water (membrane labeled sPEEK_P, P for Pristine), then hydrothermally treated in liquid water at 80°C for 72h (sPEEK_NS, NS for NanoStructured) to improve nanophase separation[59,60]. The membranes were then swollen for 24 hours in an acidified (acetic acid addition down to pH=4) water / ethanol mixture (50/50 and 64/36 volume composition) to condition the membranes prior to SG impregnation.

Solutions of SG precursors in the same solvent mixture as the one used for membrane swelling were prepared separately (stirred for 2 hours) to obtain a homogeneous solution. Hydrolysis of the SG precursors took place during this step. Then, the membranes were immersed into this solution.

Herein, the insertion of the SG phase into the host sPEEK membrane is quantified either as the membrane's weight increase ratio labeled "SG uptake" (SG_{Upt} corresponding to the weight ratio of the SG phase to the sPEEK_NS membrane used to prepare the hybrid membrane), or as the ratio of inserted SG *vs* insertable SG (considering that all the MPTMS would have condensed in sPEEK) labeled "MPTMS insertion ratio" ($MPTMS_{Ins}$):

- The SG uptake:

  $$SG_{Upt} = \frac{mSG_{dry}}{m\ sPEEK\_NS_{dry}} \times 100\% = \frac{mHyM_{dry} - m\ sPEEK\_NS_{dry}}{m\ sPEEK\_NS_{dry}} \times 100\% \quad \text{(eq. 1)},$$

  where mSG_{dry}, $mHyM_{dry}$, $msPEEK\_NS_{dry}$, are the mass of the SG phase in the hybrid membrane, the mass of the hybridized sPEEK and sPEEK_NS membranes respectively, in the dry state.
- The MPTMS insertion ratio:

  $$MPTMS_{Ins} = \frac{mSG_{dry}}{mSG_{dry}\ \text{insertable (assuming a complete insertion)}} \times 100\% \quad \text{(eq. 2)}$$

After various impregnation times (1 to 144 hours at 30°C), the membranes were removed from the solution and dried in an oven under a nitrogen flux at room temperature overnight prior to a post condensation step (PC) of 24 hours at 70°C and a relative humidity (R.H.) of 6.3% to achieve a high SG phase condensation. Finally, an additional hydrothermal Post Treatment step (PT) (72 h at 80°C in liquid water) was applied to elute uncondensed SG

oligomer [61] before FC operation. The hybrid membranes are labeled: HyM-X%-I, PC or PT where X is the SG uptake and I, PC or PT stand for the last step of elaboration (I = impregnation, PC = post condensation, PT = hydrothermal post treatment).

2.3 Hybrid membrane characterization

Gravimetric measurements: SG and water uptake

-SG uptake: the SG_{Upt} (eq. 1) of the hybrid membrane was calculated from gravimetric measurements of the mass of sPEEK_NS ($msPEEK\_NS_{dry}$) and mass of the hybrid membrane ($mHyM_{dry}$), in the dry state.

-water uptake: The hybrid membrane water uptake (W_{Upt}) in liquid water at 25°C was calculated as follows:

$$W_{Upt} = \frac{mHyM_{wet} - mHyM_{dry}}{mHyM_{dry}} \times 100\% \qquad \text{(eq. 3)}$$

To measure the mass of the water swollen hybrid membrane, $mHyM_{wet}$, excess water on surfaces was removed from the membrane using absorbent paper just before weighing.

Confocal Raman spectroscopy: confocal Raman spectroscopy was performed in backscattering mode using a LabRam HR (Laser He Ne-632.8 nm-17 mW) from HORIBA Jobin Yvon, with a 100x long working distance objective and an X, Y micro-motorized stage. Calibration was performed following the standard procedure from Horiba using a silicon sample (zero order and sine bar corrections). Data were treated using LabSpec Software version 6.3.40. The analyzed range was from 400 to 3250 cm^{-1} with a grating of 600 gr/mm, a hole of 200 µm and a slit of 100 µm. The acquisition time was 12 seconds with 4 accumulations per spectrum. To avoid photothermal polymer degradation by the laser beam, a ND filter of 25% was used.

NMR measurements: high-resolution solid-state ^{13}C, ^{29}Si and ^{1}H NMR spectra were recorded with a 4 mm Bruker CPMAS probehead on a Bruker AVANCE DSX 500 spectrometer operating at 127.7 MHz for the ^{13}C, 99.4 MHz for the ^{29}Si and 500.18 MHz for the ^{1}H. The 4 mm (92 µL) diameters cylindrical double bearing rotors made of zirconia were

rolled up on themselves in order to fill the maximum of rotor volume. The chemical shifts values were calibrated using the glycine carbonyl signal, set at 176.03 ppm for the ^{13}C and to the Q8M8 Q_4 most right signal set at -109.7 ppm for the ^{29}Si, both relative to the tetramethylsilane (TMS). MAS spinning speed was set to 8 kHz. No faster spinning rate was used because of the inhomogeneity of the material inside the rotor. For the 1D CPMAS spectra a ^{1}H RF field strength of 100 kHz was used for proton pulses (90° pulse duration of 2.5 µs) and for heteronuclear dipolar decoupling. For the cross-polarization step, a ramped rf field centered at 82 and 77 kHz was applied on protons for ^{13}C and ^{29}Si CPMAS spectra, respectively. The ^{13}C and ^{29}Si field strengths were set to match the Hartman–Hahn condition during CP experiment. For each CPMAS spectrum, 5000–16,000 transients were accumulated with a CP contact time of 2 ms for the ^{13}C and of 3.5 ms for the ^{29}Si and a recycle delay of 5-6 s for both nuclei. Nonquaternary suppression (NQS) experiments were performed by intervalling the 40 µs delay with zero field strength before the acquisition period in the 13C CP experiment[62].

In the 2D HETCOR experiment[63] data were collected with 36 data points in the ^{1}H dimension and 1992 data points in the ^{13}C dimension. The corresponding spectral widths were 12 and 50 kHz, respectively. For each t_1 increment 1638 scans were accumulated with a recycle time of 4s. For the cross-polarization step, a ramped rf field centered at 82 and 77 kHz was applied on protons for ^{13}C, respectively, while the carbon and silicon rf field were matched to obtain optimal signal. During acquisition, the proton decoupling field strength was also set to 100 kHz. The spinning frequency was 8 kHz and the contact time for the cross-polarization step set to 2 and 3.5 ms for ^{1}H-^{13}C and ^{1}H-^{29}Si experiments, respectively. Quadrature detection in ω_1 was achieved using the States method.

The interest of using such a method is proven for example in[64–66]. For the 1D and 2D experiments, the corresponding sequences are those of TOPSPIN, the NMR software proposed by Bruker Corporation.

Dynamic Vapor Sorption balance: The water sorption isotherms were recorded using a DVS1000-Org instrument from Surface Measurement Systems (SMS, London, UK). The vapor partial pressure was controlled by mixing dry and water saturated nitrogen, using electronic mass flow controllers. The experiments were carried out at 25°C increasing the relative humidity by step of 0.1 from 0 to 0.9. Prior to measurements, the samples were dried at 25°C under dry nitrogen until a constant weight. The equilibrium was considered to be

reached when changes in mass versus time (dw/dt) were lower than 0.005% for ten consecutive minutes (2000 minutes for the drying step). From the last step 0.95 (95% RH), the water desorption isotherms were recorded in the same conditions.

Thermogravimetric Analysis (TGA): The SG uptake (after aging tests) of the hybrid membrane and the thermal stability were obtained from thermogravimetric analysis (TG 209 F3 TARSUS from NETZSCH). For thermal stability evaluation, samples were heated under O_2 flow (40 mL/min) at 10ºC/min from room temperature up to 700ºC. For SG uptake measurements after aging tests, samples were heated under O_2 flow (40 mL/min) at 10ºC/min from room temperature up to 475ºC to reach the degradation temperature of the organic phase. Then an isothermal step of 35 min at 475°C was used to eliminate slowly enough the organic phase without flushing any SiO_2 residue out of the alumina crucible with the combustion gases. Finally, the sample was heated at 20°C/min up to 700°C to finish the combustion of the organic phase. The amount of SG phase (SG uptake before aging, remaining SG content after aging) was determined according to equation 4 considering the SiO_2 weight residue at 700°C and the weight of dry hybrid membrane at 200°C (a temperature corresponding to the complete water desorption, before any decomposition of the organic phase).

$$SG_{Upt\ TGA} = \frac{\frac{m\ SiO2\ residue\ at\ 700°C}{MSiO_2} \times MSG}{m\ HyM\ at\ 200°C - \frac{m\ SiO2\ residue\ at\ 700°C}{MSiO_2} \times MSG} \times 100\% \qquad \text{(eq. 4)}$$

where M SiO_2 = 60.08 g/mol and MSG = Molar Mass of the SG repeat unit of the condensed SG phase = 127.2 $g.mol^{-1}$. It should be stressed that the hybrid membrane mass at 200°C obtained by TGA is slightly lower (the hybrid membrane is dryer) than the one obtained after overnight drying in an oven under a nitrogen flux at room temperature, and therefore $SG_{Upt\ TGA}$ (eq. 4) is slightly higher than SG_{Upt} (eq. 1).

Proton Conductivity: The in-plane proton conductivity was measured by impedance spectroscopy using Material Mates 7260 Frequency Response Analyzer and a home-made conductivity cell. The cell is composed of two blocks of polymer support holding series of 1 mm thick gold electrodes spaced from 0.25 cm to 1.75 cm. The spectra were obtained between 100 Hz and 5 MHz at room temperature and at the swollen state, after equilibrium (at least 24 hours in liquid water).

The proton conductivity was calculated according to equation 5:

$$\sigma = \frac{L}{W \times e \times R} \quad \text{(eq. 5)}$$

Where L is the distance between gold electrodes, W is the membrane width and *e* is the membrane thickness. R is the membrane resistance. This resistance was determined from the high-frequency intercept of the impedance with the real axis[67].

Gas transport properties: Gas permeability coefficients were determined at 20°C for H_2, He and CO_2. The permeation cell consisted of two compartments separated by the studied membrane. The effective membrane area was 3 cm^2. The cell was thermostated at 20 ± 1°C. A preliminary high vacuum desorption was realized to ensure that the static vacuum pressure changes in the downstream compartment were smaller than the pressure changes due to gas diffusion. Then a 3 bar gas pressure was introduced in the upstream. The increase of pressure in the downstream compartment was measured with a 10 torr datametrics pressure sensor, allowing determining the gas flow (*J*) through the membrane. The permeability coefficient *Pe*, expressed in barrer unit (1 barrer = $10^{-10}$$cm^3$(STP).cm.$cm^{-2}$ s^{-1} $cmHg^{-1}$= 7.5 x 10^{-18} Nm^3.m.m^{-2}.s^{-1}.Pa^{-1}= 3.348 10^{-16} mol.m.m^{-2}.s^{-1}.Pa^{-1}), was calculated from the gas flow in the steady-state (J_{stat}) according the following law:

$$P_e = \frac{eJ_{stat}}{\Delta P} \quad \text{(eq. 6)}$$

where *e* is the thickness of the membrane and *ΔP* is the pressure gradient.

2.4 Membrane chemical stability

Accelerated aging test: To evaluate the efficiency of the SG phase to mitigate oxidative attacks, accelerated aging tests were performed in H_2O_2 solutions (prepared by mixing 30 wt% H_2O_2 solution with pure water, without ferrous additives to avoid ionic exchange with the membrane). Therefore, the chemical attacks were thermally activated at 80°C for 24 h. The aging was controlled by the H_2O_2 concentration (ranging from 0.02 to 0.5 wt%) while keeping a constant volume of oxidizing solution (2 mL) per mg of dry hybrid membrane. This range of

concentrations was determined from the amount of H_2O_2 necessary to oxidize a model molecule similar to the sPEEK repeating unit[54] and was found adapted to sPEEK membranes (0.5 wt% resulting into a strong aging of sPEEK_NS with membrane fragmentation).

Quantification of the extent of degradation: The extent of degradation of the sPEEK phase of the hybrid membrane was measured by UV-Visible (UV absorption at 295 nm characteristic of sPEEK degradation products found in the oxidizing solution after aging tests), but also by swelling measurements of the membrane (gravimetric), its weight loss (measured after drying), and the TGA determination of the relative amounts of the SG vs sPEEK phases after aging ($SG_{Upt\ TGA}$).

2.5 Membrane operability in fuel cell

Membrane Electrodes Assemblies (MEA) were made according to the following protocol (for Nafion, sPEEK and hybrid membranes):

- Membranes were inserted between two 235 µm Gas Diffusion Electrodes (GDE) from Baltic FuelCells GmgH made from Sigracet SGL 28BC gas diffusion layers with a micro-porous layer. The GDE Pt loading was 1 $mg.cm^{-2}$ to limit activation losses. The two GDE were carefully aligned on both sides of the membrane.
- These sets of membrane and GDE were then cold pressed at ambient temperature 3.5 minutes at a pressure of 5.5 MPa (to slightly pre-assemble the membrane and electrodes for easier handling).
- Then, the whole MEA was placed in a perforated polyamide bag for a nitrogen sweep of 30 minutes to remove oxygen before hot pressing to avoid a pre-oxidation of the stabilizing groups.
- Finally, the MEA were hot pressed 3.5 minutes at 135°C and 6.2 MPa in the bag with a continuous nitrogen sweep.

The MEAs surface was 7,22 cm^2 (19×38 mm). MEAs were tested in a single cell with identical gold-coated brass plates with a single serpentine channel (19 passes) of 0.7 mm in depth and 1 mm thick on the anode and cathode sides. The width of the channel rib was 1

mm. The anode and cathode flow field plates were assembled together using four M6 bolts tightened to 5 Nm. The plates were then inserted between two stainless steel plates thermostated to 70°C.

Before the aging test, MEAs were subjected to a conditioning and break-in stage consisting in:

- 20 minutes temperature rise from 40°C to 70°C, feeding the anode with 10 slph of hydrogen while flushing the cathode with 10 slph of nitrogen.
- 2 hours of constant voltage operation according to the following sequence: 0.6 V (45 seconds), open circuit (30 seconds) and 0.3 V (60 seconds).

Gas supply during the constant voltage operation stage was identical to that of the aging test, i.e. pure hydrogen and oxygen at 80% RH with a stoichiometry equal to 1.5 on both sides.

During the aging test, the MEA were operated 120 hours at a current density of 0.55 A/cm² and a full characterization sequence was performed every 12 hours: 1) measurement of electrochemical impedance spectra (EIS) at 0.5 A/cm² and polarization curves, 2) cathode compartment flushed with nitrogen, 3) potentiostatic EIS measurements and cyclic voltammetry used to assess the platinum ElectroChemical Surface Area (ECSA) by cycling the potential between 0.1 and 0.8 V at a sweep rate of 50 mV/s. We also measured the hydrogen permeation current by setting the cell voltage to 0.5 V.

3 Results and discussion

3.1 Membrane elaboration

3.1.1 Impregnation conditions

The SG phase must be introduced in sufficient amount to reach the desired lifetimes but without excess, in order to avoid degrading the functional properties. Controlling the amount of SG phase in the resulting hybrid membrane is therefore critical.

In order to define the optimal conditions of impregnation, we first studied the impact of the SG precursor concentration in the impregnation solution [MPTMS] on the SG insertion ratio (into the sPEEK membrane) labeled $MPTMS_{Ins}$ (eq.2). Figure 1 presents the results obtained for precursor's concentrations ranging from 0.0042 to 0.2 mol/L. These impregnations were carried out on pretreated sPEEK membranes (nanostructuring process of 72 h at 80°C in liquid water[59]) (sPEEK_NS) after a swelling in an acidified water / ethanol mixture. 104 mL of solution per gram of membrane were used, for 96 h of impregnation at 30°C.

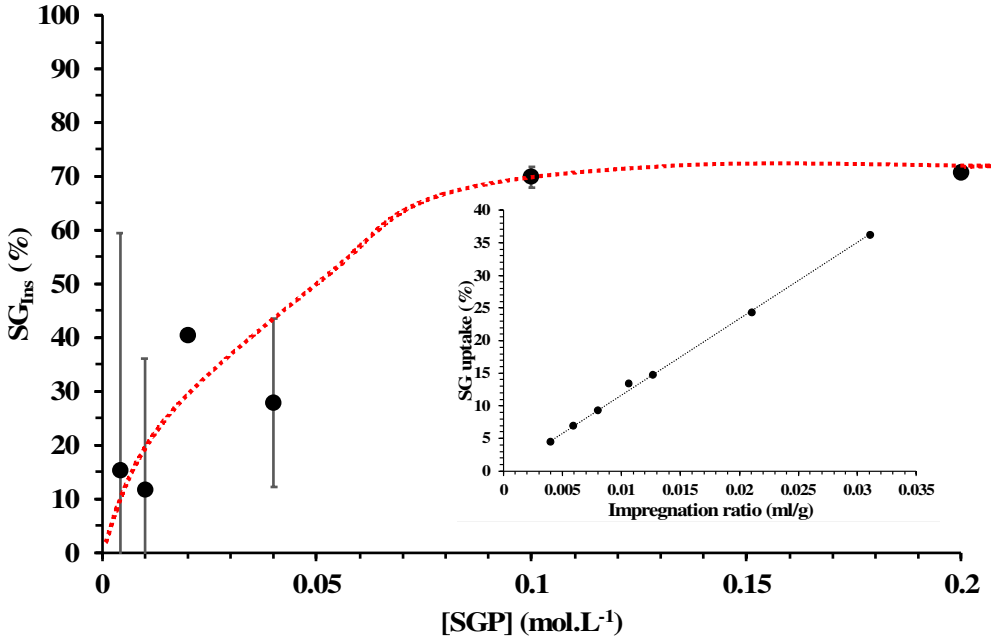

Fig. 1.

Evolution of the $MPTMS_{Ins}$ with the [MPTMS] (104 mL of solution per gram of membrane, 50/50 vv water/ethanol, 96 h of impregnation at 30°C) (eye guide curve in red) (insert: SG_{Upt} as a function of the Impregnation Ratio [MPTMS] = 0.1 mol/L, 64/36 vv water/ethanol, 30 h of impregnation at 30°C, $MPTMS_{Ins} \geq 90\%$).

One can see that $MPTMS_{Ins}$ increases with [MPTMS] up to a maximum value of about 70% reached for a concentration of 0.1 mol/L. From this observation we can understand that at low concentration of MPTMS, the diffusion/condensation process is less efficient than for higher concentrations. The diffusion of MPTMS in the membrane comes from the gradient of concentration of the MPTMS between the solution and the sPEEK membrane (osmotic pressure), the higher the concentration in the solution, the higher the gradient. However simple calculation shows that the MPTMS insertion ratio does not correspond to the equilibrium of concentration between the surrounding solution and the membrane. Indeed,

according to the membrane swelling, the insertion ratio should be far below the values reported on Figure 1 (with a $MPTMS_{Ins}$ maximum value of about 3%, see supplementary material S1). This clearly indicates that MPTMS diffuses into the membrane where it condenses to form the SG phase. The concentration gradient is restored as MPTMS condenses in the membrane, allowing additional MPTMS to diffuse into the membrane. The effectiveness of this diffusion/condensation process is favored by the impregnation conditions chosen. Indeed, the slightly acidic pH of the impregnation solution (pH = 4) promotes the hydrolysis of MPTMS in the solution while limiting the self-condensation. Conversely, this self-condensation is favored in the host membrane due to its very high acidity (pH << 1).

One can observe on Figure 1 that $MPTMS_{Ins}$ reaches a maximum plateau of about 70% beyond a concentration of 0.1 mol/L. This corresponds to a SG uptake of about 90% for 0.1 mol/L and 185% for 0.2 mol/L (higher concentration studied), *i.e*, a SG phase representing almost 1/2 and 2/3 of the mass of the hybrid membrane respectively. This plateau should be related to the sPEEK mechanical resistance that does not allow for infinite SG insertion (otherwise the SG insertion should continue rising with [MPTMS] due to the increasing osmotic pressure) but also to the dilution of the acid functions due to the incorporation of the SG phase (dilution decreases acidity which impedes the SG condensation).

Obviously, the synthesis conditions offering the best MPTMS insertion ratio have to be chosen to be able to control the SG uptake of the sPEEK membrane and to lower the cost of the process. Therefore, the [MPTMS] was fixed at 0.1 mol/L for the rest of the study, larger concentrations corresponding to impractical (very low) volumes of impregnation solutions for SG uptakes of 10, 20 or 30%.
We then studied the impact of the volume fraction of ethanol on the swelling of the sPEEK_NS and found that a 64/36 vv water/ethanol composition was ideal to avoid an overswelling and therefore membranes' wrapping. It was also shown that the impregnation time could be limited to 30h instead of 96h without any detrimental effect (see supplementary material S2).

After optimizing the MPTMS concentration and the impregnation time (fixed respectively at 0.1mol/L and 30h) the strategy was naturally to vary the volume of MPTMS solution per gram of membrane (a ratio labeled the Impregnation Ratio and expressed in mL/g) to control the amount of inserted SG phase in the hybrid membrane.

By varying the Impregnation Ratio from 0.0004 to 0,032 mL/g we obtained hybrid membranes with a SG_{Upt} ranging from 5 to 30%.

One can observe on the insert of Figure 1 a linear variation of the SG_{Upt} with the Impregnation Ratio. From this observation, we can conclude that a simple adjustment of the Impregnation Ratio (amount of SG precursor solution per gram of sPEEK membrane) makes possible an easy and robust control of the SG_{Upt} of a sPEEK membrane while maintaining an excellent $MPTMS_{Ins}$.

3.1.2 Optimization of the extent of polycondensation of the SG phase

We studied by ^{29}Si NMR the evolution of the degree of condensation of the SG phase after each step of the process, as presented in Figure 2.

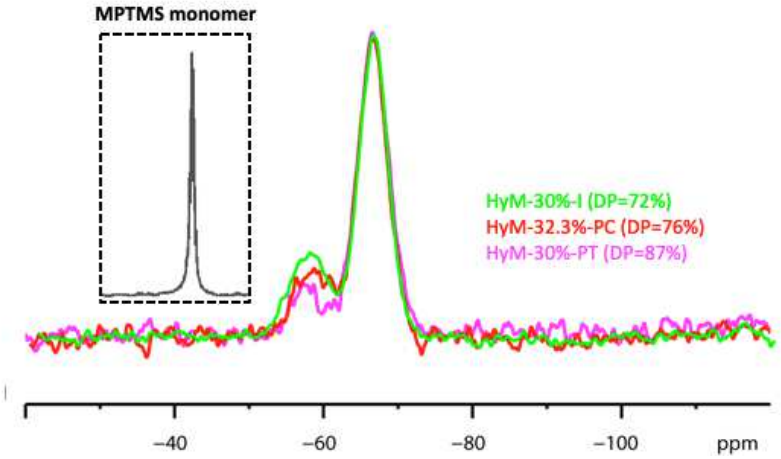

Fig. 2. CPMAS solid ^{29}Si NMR analysis of a hybrid membrane with a SG_{Upt} of 30% after the three steps of the process: impregnation (I), post-condensation (PC) and hydrothermal post treatment (PT). Normalized spectra with respect to the T3 peak (-68.4 ppm). The insert corresponds to the MPTMS monomer (T0).

The spectra obtained were normalized with respect to the peak labeled T3 [C–Si(OSi)$_3$] at -68.4 ppm characteristic of the Si atoms having reached their maximum degree of condensation (3 siloxane bonds per repeating unit, one for each hydrolysable group of the MPTMS). A second peak, labeled T2 [C–Si(OH)(OSi)$_2$] is detected at -58.2 ppm and is characteristic of Si atoms with only two siloxane bonds. The absence of T1[C–Si(OH)$_2$(OSi)] peak at -48.4 ppm and T0 [C–Si(OH)$_3$] peak at -42.7 ppm shows that no dimer or

uncondensed MPTMS are found in the membrane at the end of the impregnation step. Therefore, the extent of condensation of the SG phase (labeled ExtC) can be expressed as the ratio T3/(T2+T3). An ExtC of 100% corresponding to 100% of T3 and an ExtC of 0% corresponding to 100% of T2. From the three NMR spectra of Figure 3, an ExtC of 72% was found after I, 76% after PC and finally 87% after PT, increasing as we proceed through the elaboration steps.

If the increase of ExtC from I to PC can be attributed to an increase of the T3 signal, the ExtC increase from PC to PT was found to correspond to a decrease of the T2 signal. Indeed, we measured the elution of about 3 wt% of the SG phase after the PT step, which corresponds to the oligomers not completely condensed in the SG phase after PC (and therefore giving a T2 signal by RMN). The PT step that swells the hybrid membrane in water at 80 °C is therefore useful to wash out leachable oligomers that could poison the FC catalyst during operation. An unexpected result is the structuring effect of the sPEEK phase on the SG phase. Indeed, the MPTMS phase inside the host membrane is a more regular material compared to the one obtained by *ex-situ* condensation (supplementary material S3). In addition, if a partial oxidation of the SH groups is induced during the manufacturing process, the SG phase remains reactive/protective as these groups have not reached their final state of oxidation (supplementary material S3).

3.1.3 Distribution of the SG phase in the host sPEEK membrane

To study the distribution of the SG phase within the membrane confocal Raman analysis was performed on a cryo-ultramicrotomed cross-section (not the ultrathin section but the opened membrane). The cryo-ultramicrotomy procedure used to prepare the sample provided access to very smooth and unmodified cross-section (no compressive forces, no shearing) [68], avoiding the use of autofocus during Raman mapping [61].

The distribution of the SG phase inside the membrane was accessed through the ratio between the area of the SG phase peak (between 2800 and 3015 cm^{-1} aliphatic CH) and sPEEK contributions (between 3020 and 3130 cm^{-1} aromatic CH), hereby called $R_{SG/sPEEK}$ after background correction. The complete Raman assignment of the bands relative to the sPEEK and the SG phase is shown in supplementary material (S4). The SG phase distributions across three hybrid membranes HyM-5.1%-PT, HyM-19.3%-PT and HyM-29.5%-PT are presented in Figure 7. One can observe that the SG uptake over a thickness of about a micrometer on

both sides of the membranes is lower than in the bulk, whatever the SG uptake. It is important to outline that no additional treatment (like a surface cleaning) was applied after SG impregnation which could explain the formation of this depleted zone. It has been observed from the impregnation step and was not created during the PT step. We assume that it could originate from a difference of morphology between the surface of the sPEEK membranes *vs* the bulk, that would limit the amount of SG that the sPEEK membrane can accept at the surfaces. This point could be investigated for example by X-ray diffraction with a micro X-ray beam scanning the membrane across its thickness[69].

As observed in Figure 3, the SG phase appears homogeneously distributed in the rest of the sPEEK membrane. Mauritz *et al.*[70] and Klein *et al.*[49] reported a reversed profile for SG hybrid membranes based on Nafion (greater SG content near the outer surfaces and minimum SG content in the middle of the membrane). They had to clean the surfaces of the hybrid membranes with alcohol after impregnation to avoid the formation of pure SG skins. The difference between these host membranes may come from the difference of acidity of the sulfonic groups (much more acidic for Nafion than for sPEEK), the difference of water uptake of the membranes (three times higher for sPEEK_NS than for Nafion) and the differences of membrane chemistries/chemical affinity (aromatic *vs* fluorinated) with respect to the MPTMS.

All these parameters lead to a much faster condensation of the MPTMS at the surface of the Nafion membrane[71], which prevents a uniform MPTMS diffusion in the rest of the membrane.

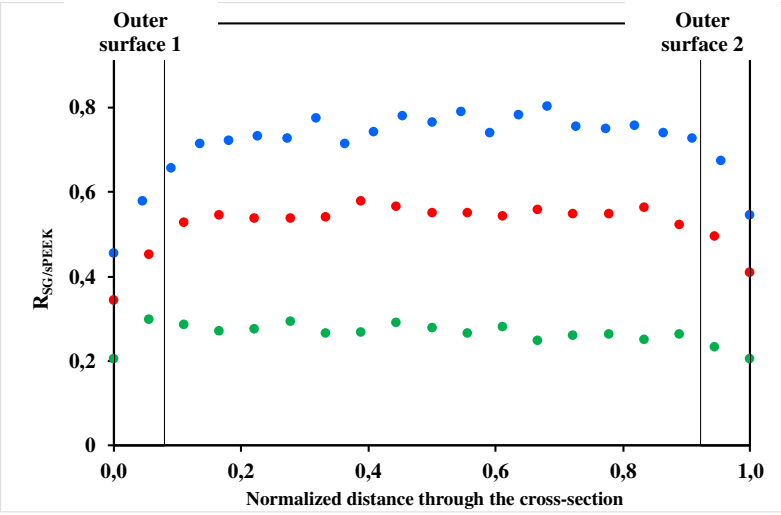

Fig. 3. Relative amount of SG phase through the membranes' cross-sections (area ratio between the bands between 2800 and 3020 cm^{-1} and the band between 3020 and 3130 cm^{-1})

for hybrid membranes HyM-5.1%-PT (● - membrane thickness = 19µm), HyM-19.3%-PT (● – membrane thickness = 18µm) and HyM-29.5%-PT (● - membrane thickness = 22µm).

In the supplementary material (S5) we present the corresponding AFM modulus imaging of cryo-ultramicrotomed cross-sections of sPEEK-NS, HyM-5.1%-PT, HyM-19.3%-PT and HyM-29.5%-PT. The morphology of the membranes confirms the Raman observations.

3.2 Functional properties

3.2.1 Water sorption

The water content strongly impacts the membrane properties, such as its proton conductivity, mechanical properties and dimensional stability. Thus, the moisture and liquid water sorption of the sPEEK_NS and the hybrid sPEEK membranes with SG uptake ranging from 10 to 30 % were studied.

The water sorption isotherms are reported in Figure 4 respectively for sPEEK-NS membranes and hybrid membranes HyM-9.8%-PT, HyM-20.4%-PT, and HyM-31,7%-PT. We observe the typical sigmoidal sorption isotherms of ionomers[56]. The downward concavity observed at low RH can be related to the binding of the strongly interacting first shell of water molecules to hydrophilic groups, while the upward concavity observed at high RH is mainly due to binding of water molecules in the formation of additional solvated shells (*i.e* 'free' water) and to water clusters.

As expected, we observe that the nanostructuring effect induced by the hydrothermal treatment (going from sPEEK_P to sPEEK_NS) leads to a significant increase of water sorption of the membrane (supplementary material S6). When comparing the isotherms obtained for sPEEK_NS with those of hybrid membranes (Figure 4), it is clear that the water sorption decreases as the SG uptake increases. However, if the water sorption is expressed as the weight percentage of water molecules sorbed per sulfonic acid groups (insert of Figure 4), the water sorptions are found equivalent for sPEEK and hybrid membranes. This suggests that, the polysiloxane phase does not hinder the accessibility of the ionic SO_3H groups and exhibits itself a limited water sorption. As a reminder relatively lower diffusion coefficient of water are found for polyaromatic membranes compared to PFSA[72].

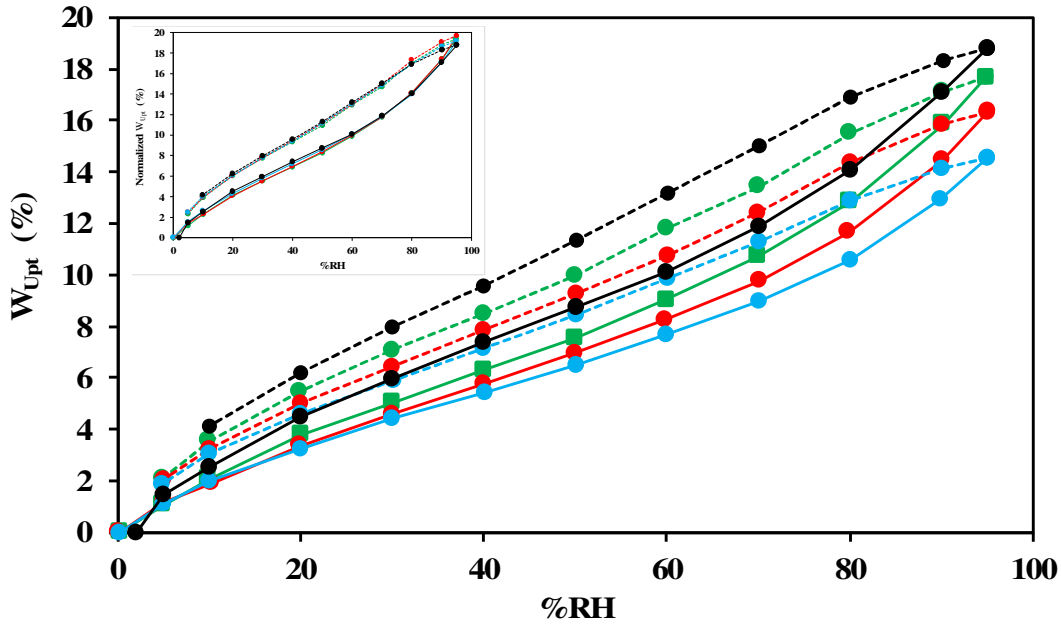

Fig. 4. Water sorption (—)/ desorption (---) isotherms recorded on sPEEK_NS (●) and hybrid membranes: HyM-9.8%-PT (●), HyM-20.4%-PT (●), and HyM-31,7%-PT (●) (Insert: isotherms normalized according to the mass of sPEEK phase)

A different trend is observed for the liquid water uptake and the proton conductivity of membranes measured in the swollen state at room temperature (after 72 hours at 80°C in liquid water to be closer to the membrane's state during FC operation). As we can observe in Table 1, the addition of about 5% of SG phase leads to an increase of more than 30% of the water uptake (135 *vs.* 101%) and of the proton conductivity (115 *vs.* 88 mS.cm^{-1}) of the hybrid membrane HyM-4.4%-PT whereas its calculated IEC is 5% lower than the one of sPEEK_NS (1.28 *vs* 1.34). For HyM-17.5%-PT the water uptake and the proton conductivity stay higher or equivalent to that of sPEEK_NS, when they both finally slightly decrease below the values of sPEEK_NS for HyM-29.3%-PT. These results are very promising as a limited addition of SG phase (4.4%) shows positive impact on both water uptake and proton conductivity.

Sample	SG_{Upt} (%) (±0.1%)	IEC♠ (meq.g^{-1})	Water uptake (W_{Upt}%) at room temperature after 72h/80°C (%) (± 2%)	H^+ conductivity at room temperature after 72h/80°C (mS.cm^{-1}) (± 5%)

sPEEK_P	×	1.34	×	31♣
sPEEK_NS	×	1.34	101	88
HyM-4.4%-PT	4.4	1.28	135	115
HyM-17.5%-PT	17.5	1.14	112	90
HyM-29.3%-PT	29.3	1.04	98	84

Table 1: SG uptake, SG mass content, IEC, water uptake and proton conductivity of sPEEK and hybrid membranes.

♣ after 96 h in liquid water at room temperature

♠IEC values from Fumatech for sPEEK and calculated for hybrid membranes

3.2.2 Gas Permeability

The gas permeability coefficients were determined in anhydrous state for membranes with SG uptakes ranging from 0 to 30%. The permeability data are reported in Table 2 for He, H_2 and CO_2. The range of gases was chosen in order to vary their polarity and their kinetic diameter.

Sample	sPEEK_P	sPEEK_NS	HyM-7.2%-PT	HyM-9%-PT	HyM-19.3%-PT	HyM-27.1%-PT
He (barrer) (±7%)	3.45	3.92	4.05	4.19	4.76	4.22
H_2 (barrer) (±7%)	2.44	2.752	2.79	2.87	3.38	2.94
CO_2 (barrer) (±7%)	0.36	0.42	0.51	0.52	0.5	0.56

Table 2: Evolution of the gas permeability coefficients as a function of SG content

Unlike polar domains, less polar regions favor gas transport in anhydrous state due to their lower cohesive energy density[73]. As the nanostructuration process led to reinforced nanophase separation between SPEEK ionic and non-ionic domains, we can assume that ionic domains interfered in a lesser extent with gas transport in the nanostructured sPEEK. Consequently, a small increase of gas permeability was observed going from pristine sPEEK membrane to nanostructured membrane.

Incorporating SG within the membrane led to an additional increase of gas permeability (slightly higher for CO_2 (around 24%) than for He and H_2 (around 9%)). It could then be concluded that the formation of the SG phase within sPEEK membrane made additional diffusion paths available for penetrants, especially for CO_2, which has higher size and polarity than H_2 and He.

It is noteworthy that for all studied membranes the gas permeability was much lower than the one measured on Nafion 112 and 212 in the same conditions (in the range 4.5-5 barrer for H_2), showing here the interest of polyaromatic membranes for FC application.

3.3 Thermal and Chemical stabilities

TGA analysis carried out under oxygen demonstrated that whatever their composition, the thermal stability of the hybrid membranes meets all the requirements of FC application (supplementary material S7).

The chemical stability of the hybrid membranes towards oxidation was studied by immersing them in H_2O_2 solutions for 24 hours at 80°C without ferrous ions (thermal activation) to avoid ion exchange with protons of the sulfonated groups of the membrane (possible physical crosslinking). Indeed, this crosslinking could reduce the membrane's swelling and therefore the membrane's aging. It could also hide the swelling resulting from chain scissions during the expected degradation of sPEEK membrane (possible overestimation of the membrane's stability). Assuming a relationship between the concentration of the H_2O_2 solution and the aging time, the accelerated aging was performed with H_2O_2 weight concentrations ranging from 0.02 to 0.5 wt%.

From Table 3, one can observe that for sPEEK and hybrid membranes the dry weight loss increases with the H_2O_2 concentration and that the dry weight loss of the hybrid membranes after 24 h in water at 80°C is very limited and compares well with the one of sPEEK_NS. The dry weight loss of hybrid membranes exposed to H_2O_2 solution clearly increases with the SG uptake, showing that the SG phase is very reactive towards H_2O_2. The dry weight loss of the sPEEK_NS seems to be very limited and much lower than the ones of hybrid membranes. However, sPEEK_NS exposed to 0.5 wt% H_2O_2 solution was broken down to fragments

making it impossible to handle (no dry weight was measured), a situation also observed for HyM-17.5%-PT and HyM-29%-PT, but not for HyM-6.1%-PT that shows better stability.

[H_2O_2] (Wt%) / Membrane	0	0.02	0.05	0.2	0.5
sPEEK_NS	2.8	2.9	2.6	4.7	-
HyM-6.1%-PT	1.9	5	6.2	6.3	10.2
HyM-17.5%-PT	2.2	7.6	13.2	-	-

Table 3: Dry weight loss (wt% ±0.1%) of the membranes after aging in H_2O_2 (24h at 80°C)

To quantify the extent of sPEEK phase degradation[54], a UV analysis of aging solutions was performed at 295 nm (found to be the position of the sPEEK degradation products absorption band). The results are presented in Figure 5.

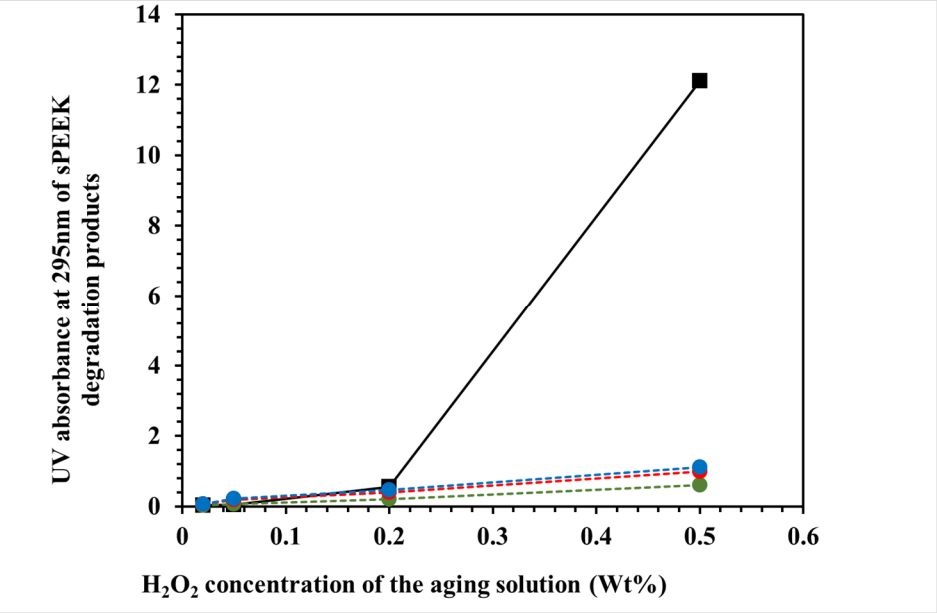

Fig. 5. The UV absorbance at 295 nm related to the sPEEK degradation products after aging of membranes sPEEK_NS (■), HyM-6.1%-PT (●), HyM-17.5%-PT (●) and HyM-29%-PT (●) is reported as a function of the H_2O_2 concentration of the aging solution. The very high absorbance for sPEEK_NS in 0.5% H_2O_2 solution was acquired after dilution of the solution (by a factor 20) in order to remain in the linear response of the spectrometer.

We can observe on Figure 5, on the one hand that the concentration of sPEEK degradation products increases exponentially with the increase of H_2O_2 concentration for sPEEK_NS.

This UV information confirms the severe sPEEK_NS degradation after the aging test at 0.5 wt% H_2O_2 (the membrane is fragmented and the aging solution was filtrated). On the other hand, at 0.5 wt% H_2O_2 the concentration of sPEEK degradation products remains much lower for hybrid membranes than what was observed for sPEEK_NS. In fact, only a linear increase of the concentration of sPEEK degradation products in the aging solution with the H_2O_2 concentration is observed for hybrid membranes. However, a clear increase of this degradation indicator is observed with the SG uptake. This may look counter-intuitive to observe a lower protection for sPEEK for higher SG uptakes. However, considering the increased weight loss observed for the hybrid membranes with the SG uptake, it can be hypothesized that HyM-17.5%-PT and HyM-29%-PT certainly become porous and expose much more the sPEEK phase to oxidizing species when compared to HyM-6.1%-PT.

From these data, we can conclude that the SG phase, being very sensitive to the oxidizing attack of H_2O_2, it efficiently protects the sPEEK phase of the hybrid membranes. However, only a limited SG uptake should be used (about 5%).

In order to confirm that the SG phase degradation is mainly responsible for the dry weight loss of the hybrid membrane (Table 3), and therefore that the sPEEK phase is protected from chemical degradation in hybrid membranes, we studied the evolution of the amount of SG phase in the hybrid membranes after aging by TGA (see Table 4).

[H_2O_2] (Wt%) / Membrane	0	0.02	0.05	0.2	0.5
HyM-17.5%-PT	14	9	-	5	-
HyM-29%-PT	36	20	-	15	-

Table 4: SG_{TGA} (wt% ±1%) measured by TGA of the membranes after aging in H_2O_2 (24h at 80°C)

Table 4 clearly highlights the fact that the SG phase is much more sensitive to oxidation than the sPEEK phase. One can observe that more than half of the SG phase is eliminated from the hybrid membrane HyM-17.5%-PT and HyM-29%-PT after 24h in a 0.2% H_2O_2 solution at 80°C.

Finally, before performing FC tests, we studied the aging impact on the water uptake as reported in Table 5. We can observe that in liquid water after 24 h at 80°C, before any aging, the hybrid membranes get more hydrated than sPEEK as follows: sPEEK_NS < HyM -29%-PT < HyM-17.5%-PT < HyM-6.1%-PT. This can be related to the higher permeability of the hybrid membranes *vs.* sPEEK suggesting a higher level of porosity (Table 2).

This seems contradictory with the water sorption results presented in Figure 4. However, it is well known that the interactions between ionomers and water may differ if water is liquid or vapor.

In addition the slight increase of the membrane porosity with the SG content seems to be counterbalanced by the fact that the SG phase is less hydrophilic than the sPEEK (as already deduced from the water sorption isotherms (Fig. 4)).

As observed in Table 5 for aged membranes, the liquid water uptake increases with aging for hybrid membranes and sPEEK_NS, as a signature of the degradation process of the SG and sPEEK phases. However a lower impact on the hybrid membranes is noticed which is probably due to the protection of the sPEEK phase thanks to the SG sacrificial phase.

[H_2O_2] (Wt%) / Membrane	0	0.02	0.05	0.2	0.5
sPEEK_NS	89	91	102	276	-
HyM-6.1%-PT	124	140	140	178	224
HyM-17.5%-PT	117	144	152	181	-
HyM-29%-PT	95	113	160	189	-

Table 5: Water uptake (wt% ±1%) of the membrane in liquid water at 25°C after aging in H_2O_2 (24h at 80°C)

3.4 Membrane operability in fuel cell

In the following, MEA aging is analyzed through linear interpolation of the evolution of the cell voltage at 0.5 A.cm^{-2} (in µV/h) over a 120 hours period. The FC tests were performed on the sPEEK_NS, hybrid membranes (HyM-4%-PT and HyM-15.7%-PT) and for comparison purpose, with Nafion 212. Figure 6 shows the polarization curves measured with all MEAs after the conditioning/break-in stage. Their performances were fully comparable at low current (below 0.25 A.cm^{-2}) while one can observe a significantly lower slope with Nafion 212 at higher currents which is, at least to some extent, probably related to the interface resistance between the GDEs and the sPEEK_NS or the hybrid membranes. EIS (potentiostatic and *operando*) also showed a much lower high frequency resistance for Nafion MEA than for sPEEK_NS or hybrid MEA (respectively 80 m Ω.cm² versus 168 mΩ.cm² and 112 mΩ.cm²), which may also be due to the better chemical affinity of the Nafion type binder used in electrode inks with the Nafion membrane than with the sPEEK membrane. In this regard, it must be noted that the membrane resistance is about 30 m Ω.cm² for sPEEK_NS and hybrid membranes (assuming a thickness of ≈ 30 µm and a conductivity of ≈ 0.1 S/cm, see Table 1) and about 50 m Ω.cm² for Nafion 212 (assuming a thickness of ≈ 50 µm and a conductivity of ≈ 0.1 S/cm). This means the membrane resistance itself accounted for *ca*. 60% of the high frequency resistance for Nafion 212 and *ca*. 20-40% with sPEEK_NS and the hybrid membranes. Of course, these values are only indicative and may vary significantly depending on the actual hydration state of the membranes, but they confirm that the main origin of the high frequency resistance is most probably linked with the quality of the membrane-electrode interface. Interestingly, the polarization curves showed better performance for the hybrid membranes than for the corresponding sPEEK membranes (respectively a current density of 1.13 and 1.07 *vs*. 0.94 A.cm^{-2} at 0.6 V).

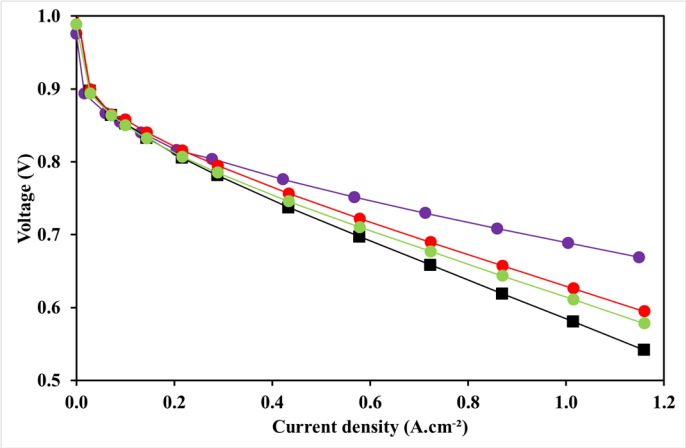

Fig. 6. Polarization curves measured with MEA made from Nafion 212 (●), sPEEK_NS (■), HyM-4%-PT (●) and HyM-15.7%-PT (●) membranes. In all cases, the MEA were assembled following the protocol described above (§ 2.5) and using 1 mgPt/cm² gas diffusion electrodes.

Figure 7 shows the evolution of the hydrogen permeation currents of the MEA with time. The hydrogen permeation currents of sPEEK_NS and the hybrid membranes MEA are remarkably low and stable compared to the one of Nafion MEA. In addition, a good agreement between *ex-situ* and *operando* permeability measurements tests is obtained. After one hundred hours of operation, we can observe a significant increase of the permeation of the sPEEK_NS membrane, a physical signature of possible membrane degradation, whereas no modification is recorded for hybrid membranes.

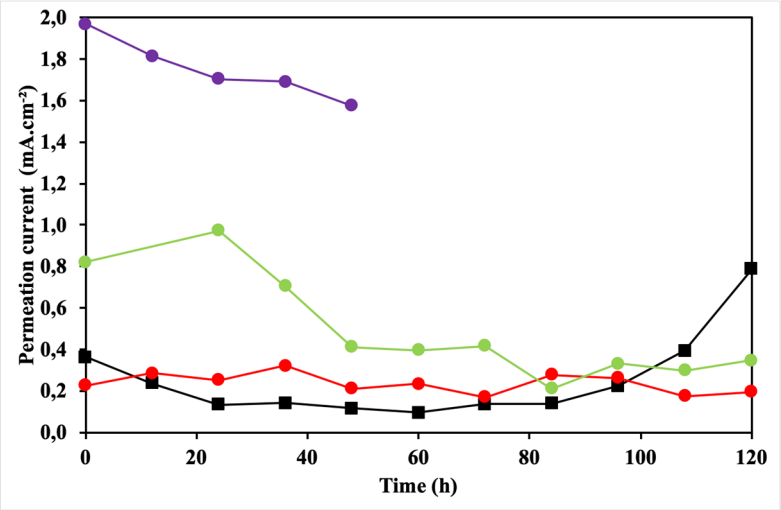

Fig. 7. Evolution of the hydrogen permeation currents measured with MEA made from Nafion 212 (●), sPEEK_NS (■), HyM-4%-PT (●) and HyM-15.7%-PT (●) membranes.

Figure 8 shows the evolution of the performance of the MEA with time (at 0.55 A/cm²). No significant variation is observed for Nafion and hybrid membranes during the 120 h of the

test, while the performance decreased significantly for the sPEEK_NS membrane. It would be premature to propose detailed interpretations of these evolutions and to this stage, this short ageing test was performed mostly to get a first assessment of the durability of the whole MEA. Phenomena such as membrane-electrodes delamination for instance, could have manifested themselves through a significant increase of the high frequency resistance, which was not observed. In the future, Accelerated Stress Tests targeting more specifically the membranes (*i.e.* OCV and/or humidity cycling) will be carried out. Nevertheless, we should stress that the sPEEK_NS and the hybrid membranes had remarkably low hydrogen permeation currents as presented above. In addition, constant value over time of their high frequency resistance, respectively 168 and 112 mΩ.cm² were measured for sPEEK_NS and hybrid membranes respectively, according to *operando* EIS. Indeed, the decrease of the performance of sPEEK_NS MEA may be explained mostly by oxygen transport issues. As a conclusion, these preliminary results demonstrate the operability of the hybrid membranes and no evidence of membrane degradation with time was observed. However, the performance of MEA made from hybrid sPEEK membranes and standard GDE using Nafion type binder need to be improved, possibly by exploring other fabrication techniques and/or optimization the ionomer content in the electrodes to decrease the interface resistances between the electrodes and the membranes.

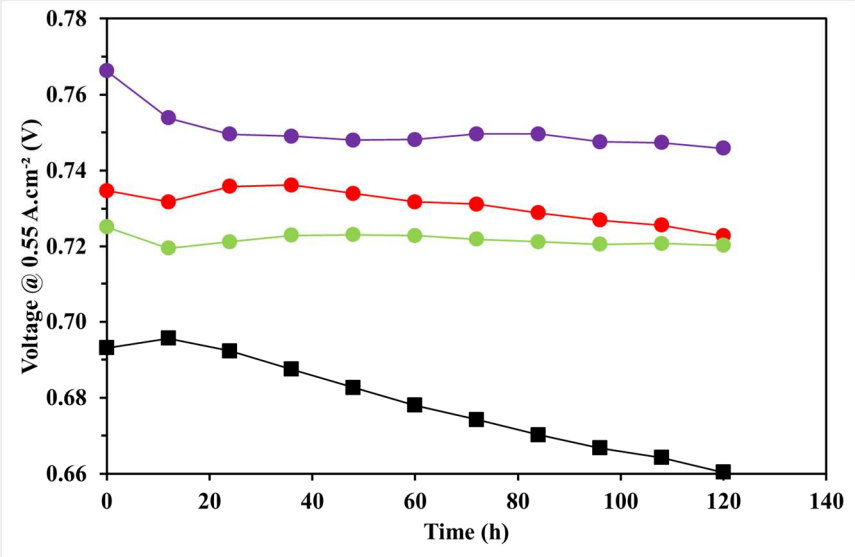

Fig. 8. Evolution of performance at I = 0.55 A/cm² of MEA made from Nafion 212 (●), sPEEK_NS (■), HyM-4%-PT (●) and HyM-15.7%-PT (●) membranes

3 Conclusions

We have presented the elaboration and properties of a new generation of proton-conducting hybrid membranes suitable for PEMFC applications. NMR and Raman analyses have shown the robustness of the fabrication process to control the SG uptake of MPTMS into sPEEK and the extent of condensation of the SG phase to prepare homogeneous hybrid membranes. The results show that, up to a SG uptake of 18% which results into a drop of about 30% of the IEC of the membrane (*vs* the pristine one), the water uptake and the proton conductivity of the hybrid membranes stay higher than the ones of the host pristine sPEEK membrane. Up to a SG uptake of 30 wt%, gas permeability of the membranes is not significantly impacted and stays much better (lower) than the Nafion's gas permeability. Accelerated aging tests and FC tests demonstrate the efficiency of the SG phase to fight against the sPEEK degradation and to improve the FC performances. Therefore, these results pave the way to developing high performance hybrid membranes fulfilling the entire requirement for high temperature/low humidity and long-term performances FC.

In a forthcoming paper, we will present the multiscale morphology of these promising membranes scrutinized by AFM and contrast variations SAXS/SANS experiments.

Acknowledgements

The authors would like to thank the Auvergne-Rhone- Alpes region of France, for providing financial support to this research work and Dr. Eric Claude from AXANE for his participation to the advisory board of this project.

Notes

The authors declare no competing financial interest.

References

[1] J. Zhang, Z. Xie, J. Zhang, Y. Tang, C. Song, T. Navessin, Z. Shi, D. Song, H. Wang, D.P. Wilkinson, Z. Liu, S. Holdcroft, High temperature PEM fuel cells, J. Power Sources. 160 (2006) 872–891. https://doi.org/10.1016/j.jpowsour.2006.05.034.

[2] A. Chandan, M. Hattenberger, A. El-kharouf, S. Du, A. Dhir, V. Self, B.G. Pollet, A. Ingram, W. Bujalski, High temperature (HT) polymer electrolyte membrane fuel cells (PEMFC) e A review, J. Power Sources. 231 (2013) 264–278. https://doi.org/10.1016/j.jpowsour.2012.11.126.

[3] A. Kraytsberg, Y. Ein-eli, Review of Advanced Materials for Proton Exchange Membrane Fuel Cells, Energy & Fuels. 28 (2014) 7303–7330. https://doi.org/10.1021/ef501977k.

[4] E. Quartarone, S. Angioni, P. Mustarelli, Polymer and Composite Membranes for Proton-Conducting, High-Temperature Fuel Cells: A Critical Review, Materials (Basel). 10 (2017) 687. https://doi.org/10.3390/ma10070687.

[5] G. Wang, Y. Yu, H. Liu, C. Gong, S. Wen, X. Wang, Z. Tu, Progress on design and development of polymer electrolyte membrane fuel cell systems for vehicle applications: A review, Fuel Process. Technol. 179 (2018) 203–228. https://doi.org/10.1016/j.fuproc.2018.06.013.

[6] R. Borup, J. Meyers, B. Pivovar, Y.S. Kim, R. Mukundan, N. Garland, D. Myers, M. Wilson, F. Garzon, D. Wood, P. Zelenay, K. More, K. Stroh, T. Zawodzinski, X.J. Boncella, J.E. Mcgrath, O.M. Inaba, K. Miyatake, M. Hori, K. Ota, Z. Ogumi, S. Miyata, A. Nishikata, Z. Siroma, Y. Uchimoto, K. Yasuda, K. Kimijima, N. Iwashita, Scientific Aspects of Polymer Electrolyte Fuel Cell Durability and Degradation, Chem. Rev. 107 (2007) 3904–3951.

[7] J. Wu, X.Z. Yuan, J.J. Martin, H. Wang, J. Zhang, J. Shen, S. Wu, W. Merida, A review of PEM fuel cell durability: Degradation mechanisms and mitigation strategies, J. Power Sources. 184 (2008) 104–119. https://doi.org/10.1016/j.jpowsour.2008.06.006.

[8] M.P. Rodgers, L.J. Bonville, H.R. Kunz, D.K. Slattery, J.M. Fenton, Fuel Cell Per fl uorinated Sulfonic Acid Membrane Degradation Correlating Accelerated Stress Testing and Lifetime, Chem. Rev. 112 (2012) 6075–6103. https://doi.org/10.1021/cr200424d.

[9] L. Dubau, L. Castanheira, F. Maillard, O. Lottin, G. Maranzana, J. Dillet, J. Perrin, E. Moukheiber, G. De Moor, C. Bas, L. Flandin, N. Caqué, A review of PEM fuel cell durability : materials degradation , local heterogeneities of aging and possible mitigation strategies, WIREs Energy Environ. 3 (2014) 540–560.

https://doi.org/10.1002/wene.113.

[10] M. Zato, J. Roziere, D.J. Jones, Current understanding of chemical degradation mechanisms of per fl uorosulfonic acid membranes and their mitigation strategies : a review, Sustain. Energy Fuels. 1 (2017) 409–438. https://doi.org/10.1039/C7SE00038C.

[11] G. Alberti, R. Narducci, M. Sganappa, Effects of hydrothermal/thermal treatments on the water-uptake of Nafion membranes and relations with changes of conformation, counter-elastic force and tensile modulus of the matrix, J. Power Sources. 178 (2008) 575–583. https://doi.org/10.1016/j.jpowsour.2007.09.034.

[12] K.D. Kreuer, On the development of proton conducting polymer membranes for hydrogen and methanol fuel cells, J. Memb. Sci. 185 (2001) 29–39. https://doi.org/10.1016/S0376-7388(00)00632-3.

[13] M. Casciola, G. Alberti, M. Sganappa, R. Narducci, On the decay of Nafion proton conductivity at high temperature and relative humidity, J. Power Sources. 162 (2006) 141–145. https://doi.org/10.1016/j.jpowsour.2006.06.023.

[14] F.M. Collette, C. Lorentz, G. Gebel, F. Thominette, Hygrothermal aging of Nafion ®, J. Memb. Sci. 330 (2009) 21–29. https://doi.org/10.1016/j.memsci.2008.11.048.

[15] J. Woo, D. Lee, M. Kim, J. Choe, S. Nam, D. Gil, Composite structures for proton exchange membrane fuel cells (PEMFC) and energy storage systems (ESS): Review, Compos. Struct. 134 (2015) 927–949. https://doi.org/10.1016/j.compstruct.2015.08.121.

[16] C. Musse, S. Sharma, M. Madalena, D.C. Forte, R. Steinberger-wilckens, New approaches towards novel composite and multilayer membranes for intermediate temperature-polymer electrolyte fuel cells and direct methanol fuel cells, J. Power Sources. 316 (2016) 139–159. https://doi.org/10.1016/j.jpowsour.2016.03.052.

[17] S. Subianto, M. Pica, M. Casciola, P. Cojocaru, L. Merlo, G. Hards, D.J. Jones, Physical and chemical modification routes leading to improved mechanical properties of perfluorosulfonic acid membranes for PEM fuel cells, J. Power Sources. 233 (2013) 216–230. https://doi.org/10.1016/j.jpowsour.2012.12.121.

[18] L. Ghassemzadeh, K.D. Kreuer, J. Maier, K. Müller, Evaluating chemical degradation of proton conducting perfluorosulfonic acid ionomers in a Fenton test by solid-state 19F NMR spectroscopy, J. Power Sources. 196 (2011) 2490–2497. https://doi.org/10.1016/j.jpowsour.2010.11.053.

[19] L. Merlo, A. Ghielmi, L. Cirillo, M. Gebert, V. Arcella, Resistance to peroxide

degradation of Hyflon® Ion membranes, J. Power Sources. 171 (2007) 140–147. https://doi.org/10.1016/j.jpowsour.2006.11.012.

[20] N. Ureña, M.T. Pérez-Prior, C. del Río, A. Várez, J.Y. Sanchez, C. Iojoiu, B. Levenfeld, Multiblock copolymers of sulfonated PSU/PPSU Poly(ether sulfone)s as solid electrolytes for proton exchange membrane fuel cells, Electrochim. Acta. 302 (2019) 428–440. https://doi.org/10.1016/j.electacta.2019.01.112.

[21] N.A. Agudelo, J. Palacio, B.L. López, Effect of the preparation method on the morphology and proton conductivity of membranes based on sulfonated ABA triblock copolymers, J. Mater. Sci. 54 (2019) 4135–4153. https://doi.org/10.1007/s10853-018-3115-5.

[22] K.H. Lee, J.Y. Chu, A.R. Kim, D.J. Yoo, Enhanced Performance of a Sulfonated Poly(arylene ether ketone) Block Copolymer Bearing Pendant Sulfonic Acid Groups for Polymer Electrolyte Membrane Fuel Cells Operating at 80% Relative Humidity, ACS Appl. Mater. Interfaces. 10 (2018) 20835–20844. https://doi.org/10.1021/acsami.8b03790.

[23] S. Magana, N. Festin, M. Fumagalli, L. Chikh, F. Gouanvé, V.H. Mareau, L. Gonon, O. Fichet, E. Espuche, Hydrophobic networks for advanced proton conducting membrane: Synthesis, transport properties and chemical stability, J. Memb. Sci. 494 (2015). https://doi.org/10.1016/j.memsci.2015.07.036.

[24] N. Festin, S. Magana, M. Fumagalli, L. Chikh, F. Gouanvé, V.H. Mareau, L. Gonon, S. Lyonnard, E. Espuche, O. Fichet, A. Morin, Morphology-induced percolation in crosslinked AMPS/Fluorolink for fuel cell membrane application, J. Memb. Sci. 534 (2017). https://doi.org/10.1016/j.memsci.2017.04.004.

[25] K. Kang, D. Kim, Toughened polymer electrolyte membranes composed of sulfonated poly(arylene ether ketone) block copolymer and organosiloxane network for fuel cell, Solid State Ionics. 335 (2019) 23–31. https://doi.org/10.1016/j.ssi.2019.02.005.

[26] N. Shaari, Recent advances in additive - enhanced polymer electrolyte membrane properties in fuel cell applications : An overview, (2019) 2756–2794. https://doi.org/10.1002/er.4348.

[27] A. Kusoglu, S. Savagatrup, K.T. Clark, A.Z. Weber, Role of mechanical factors in controlling the structure-function relationship of PFSA ionomers, Macromolecules. 45 (2012) 7467–7476. https://doi.org/10.1021/ma301419s.

[28] J. Li, X. Yang, H. Tang, M. Pan, Durable and high performance Nafion membrane prepared through high-temperature annealing methodology, J. Memb. Sci. 361 (2010)

38–42. https://doi.org/10.1016/j.memsci.2010.06.016.

[29] M.K. Hassan, A. Abukmail, K.A. Mauritz, Broadband dielectric spectroscopic studies of molecular motions in a Nafion® membrane vs. annealing time and temperature, Eur. Polym. J. 48 (2012) 789–802. https://doi.org/10.1016/j.eurpolymj.2012.01.015.

[30] W. Zhang, R. Wycisk, D.L. Kish, P.N. Pintauro, Pre-Stretched Low Equivalent Weight PFSA Membranes with Improved Fuel Cell Performance, J. Electrochem. Soc. 161 (2014) F770–F777. https://doi.org/10.1149/2.085406jes.

[31] J. Shim, H.Y. Ha, S.A. Hong, I.H. Oh, Characteristics of the Nafion ionomer-impregnated composite membrane for polymer electrolyte fuel cells, J. Power Sources. 109 (2002) 412–417. https://doi.org/10.1016/S0378-7753(02)00106-4.

[32] J. Wang, P. Li, Y. Zhang, Y. Liu, W. Wu, J. Liu, Porous Na fi on nano fi ber composite membrane with vertical pathways for e ffi cient through-plane proton conduction, 585 (2019) 157–165. https://doi.org/10.1016/j.memsci.2019.05.041.

[33] A. Rhan, K. Jane, C. Gabunada, D. Jin, Amelioration in physicochemical properties and single cell performance of sulfonated poly (ether ether ketone) block copolymer composite membrane using sulfonated carbon nanotubes for intermediate humidity fuel cells, (2019) 2974–2989. https://doi.org/10.1002/er.4494.

[34] H. Lade, V. Kumar, G. Arthanareeswaran, A.F. Ismail, Sulfonated poly (arylene ether sulfone) nanocomposite electrolyte membrane for fuel cell applications : A review, Int. J. Hydrogen Energy. 42 (2016) 1063–1074. https://doi.org/10.1016/j.ijhydene.2016.10.038.

[35] M. Tanaka, Y. Takeda, T. Wakiya, Y. Wakamoto, K. Harigaya, Acid-doped polymer nano fi ber framework : Three-dimensional proton conductive network for high-performance fuel cells, J. Power Sources. 342 (2017) 125–134. https://doi.org/10.1016/j.jpowsour.2016.12.018.

[36] R. V. Gummaraju, R.B. Moore, K.A. Mauritz, Asymmetric [Nafion®]/[silicon oxide] hybrid membranes via the in situ sol-gel reaction for tetraethoxysilane, J. Polym. Sci. Part B Polym. Phys. 34 (1996) 2383–2392. https://doi.org/10.1002/(SICI)1099-0488(199610)34:14<2383::AID-POLB8>3.0.CO;2-X.

[37] K.A. Mauritz, M.K. Hassan, Nanophase separated perfluorinated ionomers as sol-gel polymerization templates for functional inorganic oxide nanoparticles, Polym. Rev. 47 (2007) 543–565. https://doi.org/10.1080/15583720701638393.

[38] K.A. Mauritz, Organic-inorganic hybrid materials: Perfluorinated ionomers as sol-gel polymerization templates for inorganic alkoxides, Mater. Sci. Eng. C. 6 (1998) 121–

133. https://doi.org/10.1016/S0928-4931(98)00042-3.

[39] Y. Patil, S. Sambandam, V. Ramani, K. Mauritz, Perfluorinated polymer electrolytes hybridized with in situ grown titania quasi-networks, ACS Appl. Mater. Interfaces. 5 (2013) 42–48. https://doi.org/10.1021/am3017834.

[40] J. Hao, Y. Jiang, X. Gao, F. Xie, Z. Shao, B. Yi, Degradation reduction of polybenzimidazole membrane blended with CeO2 as a regenerative free radical scavenger, J. Memb. Sci. 522 (2017) 23–30. https://doi.org/10.1016/j.memsci.2016.09.010.

[41] J. Rajeswari, Z. Ziegler, G.M. Haugen, S.J. Hamrock, A.M. Herring, Investigation of Heteropolyacid Based Composite Membranes, 41 (2011) 1561–1565. https://doi.org/10.1149/1.3635688.

[42] P. Trogadas, J. Parrondo, F. Mijangos, V. Ramani, Degradation mitigation in PEM fuel cells using metal nanoparticle additives, J. Mater. Chem. 21 (2011) 19381–19388. https://doi.org/10.1039/c1jm14077a.

[43] M. Zato, J. Roziere, D.J. Jones, Mitigation of PFSA membrane chemical degradation using composite cerium oxide – PFSA nano fi bres, J. Mater. Chem. A. 5 (2017) 5390–5401. https://doi.org/10.1039/C6TA10977B.

[44] M.T. Taghizadeh, M. Vatanparast, RSC Advances nanocomposite for improving the chemical durability of proton exchange membranes in fuel cells, RSC Adv. 6 (2016) 56819–56826. https://doi.org/10.1039/C6RA07849D.

[45] A.M. Baker, D. Spernjak, S.G. Advani, K. Prasad, R.L. Borup, Zr-doped ceria additives for enhanced PEM fuel cell durability and radical scavenger stability, J. Mater. Chem. A Mater. Energy Sustain. 5 (2017) 15073–15079. https://doi.org/10.1039/C7TA03452K.

[46] Y. Yao, J. Liu, W. Liu, M. Zhao, B. Wu, J. Gu, Z. Zou, Vitamin e assisted polymer electrolyte fuel cells, Energy Environ. Sci. 7 (2014) 3362–3370. https://doi.org/10.1039/c4ee01774a.

[47] S.H. Shin, A. Kodir, D. Shin, S.H. Park, B. Bae, Perfluorinated composite membranes with organic antioxidants for chemically durable fuel cells, Electrochim. Acta. 298 (2019) 901–909. https://doi.org/10.1016/j.electacta.2018.12.150.

[48] Y. Buchmüller, Z. Zhang, A. Wokaun, L. Gubler, Antioxidants in non-perfluorinated fuel cell membranes: Prospects and limitations, RSC Adv. 4 (2014) 51911–51915. https://doi.org/10.1039/c4ra09792k.

[49] L.C. Klein, Y. Daiko, M. Aparicio, F. Damay, Methods for modifying proton exchange

membranes using the sol – gel process, Polymer (Guildf). 46 (2005) 4504–4509. https://doi.org/10.1016/j.polymer.2005.02.033.

[50] J. Jones, J. Rozière, Advances in the Development of Inorganic–Organic Membranes for Fuel Cell Applications, 2008. https://doi.org/10,1007/12_2008_150.

[51] S. Banerjee, K.K. Kar, Impact of degree of sulfonation on microstructure, thermal, thermomechanical and physicochemical properties of sulfonated poly ether ether ketone, Polymer (Guildf). 109 (2017) 176–186. https://doi.org/10.1016/j.polymer.2016.12.030.

[52] C. Perrot, L. Gonon, C. Marestin, A. Morin, G. Gebel, Aging mechanism of Sulfonated poly(aryl ether ketone) (sPAEK) in an hydroperoxide solution and in fuel cell, J. Power Sources. 195 (2010) 493–502. https://doi.org/10.1016/j.jpowsour.2009.08.001.

[53] C. Perrot, G. Meyer, L. Gonon, G. Gebel, Ageing mechanisms of proton exchange membrane used in fuel cell applications, Fuel Cells. 6 (2006). https://doi.org/10.1002/fuce.200500090.

[54] C. Perrot, L. Gonon, M. Bardet, C. Marestin, A. Pierre-bayle, Degradation of a sulfonated aryl ether ketone model compound in oxidative media (sPAEK), Polymer (Guildf). 50 (2009) 1671–1681. https://doi.org/10.1016/j.polymer.2008.12.051.

[55] M. Lavorgna, L. Mascia, G. Mensitieri, M. Gilbert, G. Scherillo, B. Palomba, Hybridization of Nafion membranes by the infusion of functionalized siloxane precursors, J. Memb. Sci. 294 (2007) 159–168. https://doi.org/10.1016/j.memsci.2007.02.032.

[56] M. Lavorgna, M. Gilbert, L. Mascia, G. Mensitieri, G. Scherillo, G. Ercolano, Hybridization of Nafion membranes with an acid functionalised polysiloxane : Effect of morphology on water sorption and proton conductivity, J. Memb. Sci. 330 (2009) 214–226. https://doi.org/10.1016/j.memsci.2008.12.070.

[57] C. Yen, C. Lee, Y. Lin, H. Lin, Y. Hsiao, S. Liao, C. Chuang, C.M. Ma, Sol– gel derived sulfonated-silica / Nafion ® composite membrane for direct methanol fuel cell, J. Power Sources. 173 (2007) 36–44. https://doi.org/10.1016/j.jpowsour.2007.08.017.

[58] H. Lin, C. Zhao, Y. Jiang, W. Ma, H. Na, Novel hybrid polymer electrolyte membranes with high proton conductivity prepared by a silane-crosslinking technique for direct methanol fuel cells, J. Power Sources. 196 (2011) 1744–1749. https://doi.org/10.1016/j.jpowsour.2010.10.003.

[59] H. Mendil-Jakani, I. Zamanillo Lopez, P.M. Legrand, V.H. Mareau, L. Gonon, A new interpretation of SAXS peaks in sulfonated poly(ether ether ketone) (sPEEK)

membranes for fuel cells, Phys. Chem. Chem. Phys. 16 (2014) 11228–11235. https://doi.org/10.1039/c4cp00710g.

[60] H. Mendil-Jakani, I. Zamanillo López, V.H. Mareau, L. Gonon, Optimization of hydrophilic/hydrophobic phase separation in sPEEK membranes by hydrothermal treatments, Phys. Chem. Chem. Phys. 19 (2017) 16013–16022. https://doi.org/10.1039/c7cp00087a.

[61] J.P. Cosas Fernandes, V.H. Mareau, L. Gonon, Co-localized AFM-Raman: A powerful tool to optimize the sol-gel chemistry of hybrid polymer membranes for fuel cell, Polymer (Guildf). 137 (2018) 231–244. https://doi.org/10.1016/j.polymer.2018.01.014.

[62] S.J. Opella, M.H. Frey, Selection of Nonprotonated Carbon Resonances in Solid-State Nuclear Magnetic Resonance, J. Am. Soc. 101 (1979) 5854–5856. https://doi.org/10.1021/ja00513a079.

[63] A.J. Vega, Heteronuclear Chemical-Shift Correlations of Silanol Groups Studied by Two-Dimensional Cross-Polarization / Magic Angle Spinning NMR, J. Am. Chem. Soc. 110 (1988) 1049–1054. https://doi.org/10.1021/ja00212a008.

[64] V. Jousseaume, A. Zenasni, L. Favennec, G. Gerbaud, M. Bardet, J.P. Simon, A. Humbert, Comparison Between E-beam and Ultraviolet Curing to Perform Porous a-SiOC : H, J. Electrochem. Soc. 154 (2007) G103–G109. https://doi.org/10.1149/1.2667980.

[65] G. Gerbaud, S. Hediger, M. Bardet, L. Favennec, Spin-coated and PECVD low dielectric constant porous organosilicate films studied by 1D and 2D solid-state NMR, J. Phys. Chem. Chem. Phys. 11 (2009) 9729–9737. https://doi.org/10.1039/b909654j.

[66] D. Lee, G. Monin, N.T. Duong, I.Z. Lopez, M. Bardet, V. Mareau, L. Gonon, Untangling the Condensation Network of Organosiloxanes on Nanoparticles using 2D 29 Si − 29 Si Solid-State NMR Enhanced by Dynamic Nuclear Polarization, J. Am. Chem. Soc. 136 (2014) 13781−13788. https://doi.org/10.1021/ja506688m.

[67] O. Savadogo, Emerging membranes for electrochemical systems Part II . High temperature composite membranes for polymer electrolyte fuel cell (PEFC) applications, Jounarl of Power Sources. 127 (2004) 135–161. https://doi.org/10.1016/j.jpowsour.2003.09.043.

[68] J.P.C. Fernandes, V.H. Mareau, L. Gonon, AFM-Raman colocalization setup: Advanced characterization technique for polymers, Int. J. Polym. Anal. Charact. 23 (2018) 113–119. https://doi.org/10.1080/1023666X.2017.1391740.

[69] H. Mendil-Jakani, R.J. Davies, E. Dubard, A. Guillermo, G. Gebel, Water

crystallization inside fuel cell membranes probed by X-ray scattering, J. Memb. Sci. 369 (2011) 148. https://doi.org/https://doi.org/10.1016/j.memsci.2010.11.059.

[70] Q. Deng, W. Jarrett, R.B. Moore, K.A. Mauritz, Novel nafion®/ORMOSIL hybrids via in situ sol-gel reactions: 2. Probe of ORMOSIL phase nanostructure by29Si solid state NMR spectroscopy, J. Sol-Gel Sci. Technol. (1996). https://doi.org/10.1007/BF00401036.

[71] U. Schubert, N. Hüsing, Synthesis of Inorganic Materials, 3rd Edition, WILEY, 2012.

[72] M.A. Hickner, Ion-containing polymers : new energy & clean water New generations of materials are being sought as solid-state, Mater. Today. 13 (2010) 34–41. https://doi.org/10.1016/S1369-7021(10)70082-1.

[73] S. Naudy, F. Colette, F. Thominette, Influence of hygrothermal aging on the gas and water transport properties of Nafion® membranes, J. Memb. Sci. 451 (2014) 293–304.

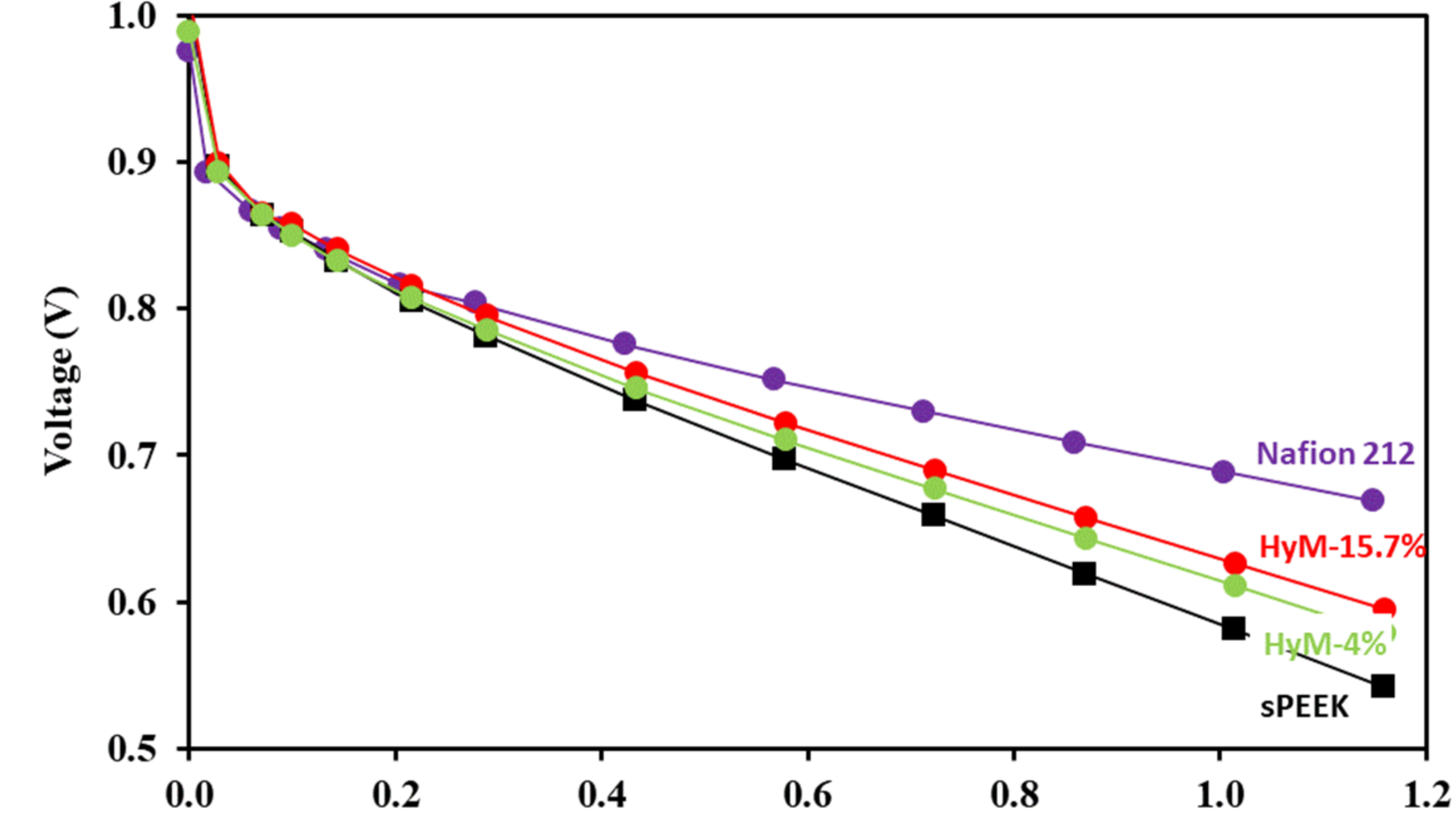
Voltage (V)
1.0
0.9
0.8
0.7
0.6
0.5
0.0
0.2
0.4
0.6
0.8
1.0
1.2
Nafion 212
HyM-15.7%
HyM-4%
sPEEK